Korean J. Chem. Eng., 39(5), 1324-1332 (2022)
DOI: 10.1007/s11814-021-0989-8

pISSN: 0256-1115
eISSN: 1975-7220

Synthesis of a fluorescence sensor based on carbon quantum dots for detection of bisphenol A in aqueous solution

Eunbi Hwang and Byunghwan Lee†

Department of Chemical Engineering, Keimyung University, 1095 Dalgubeoldaero, Dalseo-gu, Daegu 42601, Korea
(*Received 26 July 2021 • Revised 4 October 2021 • Accepted 19 October 2021*)

Abstract−In order to detect bisphenol A (BPA), one of representative endocrine disrupting chemicals (EDCs), in aqueous solution, a carbon quantum dot (CQD) was prepared using 1,3,6-trinitropyrene as a precursor by a hydrothermal synthesis method. STEM, Raman spectroscopy, FT-IR, and XPS were used for the characterization of the purified CQD (p-CD) in this work. The prepared material had a size of about 5 nm, contained many hydroxyl functional groups, and was found to have an amorphous graphene structure. In the concentration range used in this work (0 μM to 0.5 μM), p-CD showed a tendency to increase in fluorescence intensity with high linearity (R^2=0.99749) as the BPA aqueous solution concentration increased. By measuring and comparing the fluorescence excitation wavelength of p-CD and the fluorescence emission wavelength of BPA, it was found that this fluorescence change occurred by the Forster resonance energy transfer (FRET) mechanism. Fluorescence experiments were also performed using benzoic acid, hydroquinone, and naphthalene, which have similar molecular structure to BPA as comparative materials. The p-CD exhibited high selectivity for BPA detection while exhibiting a 5-fold greater change in fluorescence intensity for BPA than other target substances.

Keywords: Fluorescence Sensor, Carbon Quantum Dot, Bisphenol A, FRET Mechanism, Selective Detection

INTRODUCTION

Endocrine disrupting chemicals (EDCs) interfere with normal endocrine function by acting like hormones in the body of an organism. They are not easily decomposed in the natural environment and can exist there for a long time. Bisphenol A (BPA), a raw material for polycarbonate, is one of the representative EDCs. It has a structure similar to estrogen, a female hormone, and can interfere with the reception of the estrogen hormone and cause disorders in the endocrine system. It has been reported that BPA may cause genital dysfunction, cancer, cardiovascular disease, obesity, and diabetes. BPA leached from plastic products disposed of in landfills can flow into soil or groundwater and can also be present in the effluent of wastewater treatment plants [1,2]. This suggests the possibility that BPA exists in various environments and can disturb the ecosystem, and that people can be easily exposed to BPA from various routes without direct contact with BPA. In addition, BPA in aqueous solution can be even more dangerous. BPA may undergo an electrophilic substitution reaction with a chlorine compound in an aqueous solution to generate monochlorobisphenol A (ClxBPA), a chlorinated derivative. The estrogen activity of ClxBPA is 10 to 40 times higher than that of BPA [3]. Therefore, it is important to detect and remove trace amounts of BPA from aqueous solution.

Various detection methods, such as mass spectrometry, gas chromatography mass spectrometry, high-performance liquid chromatography, surface-enhanced Raman spectroscopy, capillary electrophoresis, electrochemical sensing, and ultraviolet-visible spectrophotometry, have been used to analyze BPA in aqueous solutions [4]. Among them, gas chromatography and liquid chromatography have the advantage of high detection sensitivity. However, these methods have some drawbacks, such as taking a long time for sample preparation, the need for specialized skills to operate the device, and expensive analysis cost [5]. Ultraviolet-visible spectroscopy is inexpensive and simple; however, detection is difficult at low concentrations due to low detection sensitivity.

In this work, fluorescent nanoparticles were used to overcome the limitations of conventional assays. Fluorescent nanoparticles have a large surface area and can cause a sensitive reaction compared to bulk particles, and are thus widely studied as detection sensors. Analyte can be detected by a change in the fluorescence signal resulting from the interaction between the analyte and the fluorescent nanoparticles. A sensor using fluorescence has the advantage of fast detection due to a fast fluorescence expression rate and a relatively high sensitivity [6]. Recently, researches on sensors that detect explosive substances, heavy metals, etc. using fluorescent nanoparticles are being actively performed. However, the synthesis of nanoparticles requires considerable energy and toxic reagents, which not only increases production costs but can cause environmental pollution. Therefore, it is important to develop eco-friendly alternative nanoparticles [7].

Fluorescent nanoparticles commonly used as sensors include quantum dots (QD), gold nanoparticles (AuNP), and carbon dots. Semiconductor QDs have high quantum efficiency and wide absorption spectrum range, so excitation can occur with a single energy source [8]. However, semiconductor QDs are made of toxic ele-

†To whom correspondence should be addressed.
E-mail: leeb@kmu.ac.kr

ments such as Cd, Se, and Te. Recently, a non-cadmium-based QD was manufactured as an alternative material, but the manufacturing method is complicated. Compared to semiconductor QDs, AuNPs have a simpler manufacturing method and high energy transfer efficiency, enabling high-sensitivity detection. However, since an organic solvent is used in the synthesis of AuNP, the synthesis process is harmful to the environment, and the manufacturing cost is high due to the nature of the raw material.

In this work, a detection sensor was prepared using carbon quantum dots (CQDs) that can compensate for the drawbacks of the inorganic fluorescent nanoparticles. CQDs are generally prepared using organic compounds such as carbohydrates, amino acids, and polymers [9]. Since it uses a carbon compound, there is little toxicity and the manufacturing cost is low. CQDs are also excellent when compared to fluorescent sensors using organic dyes, which are inexpensive and have excellent performance but can be easily photobleached. In addition, even at low concentrations, organic dyes can affect oxygen solubility in water and transmittance of visible light, thereby reducing photosynthesis, leading to environmental contamination [10,11]. Since these shortcomings can be compensated, CQDs are already being actively studied as sensors for detecting heavy metals. In addition, several studies have been carried out for detecting organic pollutants such as ascorbic acid [12], tannin acid [13], tetracycline [14], tartrazine [15,16], methylene blue [17], and glutathione [18]. However, there are relatively few researches on the detection of organic pollutants [19].

CQDs were first discovered in 2004 in the process of manufacturing and refining carbon nanotubes by arc discharge method [12]. CQDs, spherical nanoparticles with a diameter of several nanometers or less, are generally composed of carbon, oxygen, and nitrogen having a hybrid structure of sp^2 and sp^3 [10]. They have optical properties that fluoresce when irradiated with ultraviolet rays. It is known that the fluorescence properties are controlled by the quantum confinement effect and the degree of surface oxidation. The quantum confinement effect appears when the particle size is smaller than the electron-hole pair Excitone Bore radius [20]. As a result, the bandgap energy may vary depending on the size of the CQDs, which may exhibit various colors from blue to red. CQDs have a number of functional groups, such as hydroxyl, carboxyl, amine, and the like, on the surface. Depending on these functional groups, the surface oxidation degree and electronic state of the CQDs can be changed, and the emission color of the CQDs can also be changed [21]. Recently, studies on the surface modification of CQDs have also been actively conducted.

Many methods studied for the synthesis of CQDs can be classified into top-down and bottom-up methods. Top-down synthesis is a method of oxidizing bulk particles or applying energy to make particles smaller, while bottom-up synthesis is a method of growing particles from a carbon source of small molecules. Typical top-down synthesis methods include arc discharge, laser ablation, and electrochemical oxidation, but they require expensive equipment and have the disadvantage of harsh reaction conditions [22]. On the other hand, bottom-up synthesis methods such as hydrothermal synthesis and microwave irradiation are simpler and more efficient than other synthetic methods. Hydrothermal synthesis method used in this work does not require expensive equipment and can be easily accessed in a laboratory. In addition, it has good reproducibility because it does not require harsh synthetic conditions [20].

Several studies on fluorescent sensors for BPA detection using CQDs have been conducted, including gold nanoparticle complex dual emission sensors [23], silica composites using molecular imprinting techniques [24], and redox sensors that oxidize BPA with hydrogen peroxide and a catalyst [25]. The detection limits were 3.3 nM, 30 nM, and 0.4 nM, respectively, showing a low detection limit. However, the dual emission and silica composite sensors had complicated synthesis processes that took a long time because the sensor preparation processes were not performed in one-step [23, 24]. In addition, the redox sensor had the inconvenience of adding a reagent before the detection process [25]. Therefore, in this work, we attempted to manufacture a CQD fluorescence sensor that can complement the existing researches, and that the synthesis method can be made in one-step and can detect BPA by a simple method.

EXPERIMENTS

1. Reagents

For the preparation of carbon quantum dots (CQDs), pyrene ($C_{16}H_{10}$, Sigma-Aldrich, 98%, USA), nitric acid (HNO_3, Duksan, 64-66%, Korea), sodium hydroxide (NaOH, OCI, 98%, Korea), and deionized water were used. A nitrocellulose membrane filter (Sigma-Aldrich, 0.22 μm, USA) was used for the purification process, and silica 60 (0.063-0.200 mm, 70-230 mesh ASTM, Merck, Germany) and ethanol (C_2H_5OH, Samchun, 99%, Korea) were used for the silica gel column chromatography process. Deuterated chloroform ($CDCl_3$, Sigma-Aldrich, 99.8%, USA) was used as a solvent in the NMR analysis. L-tryptophan ($C_{11}H_{12}N_2O_2$, Sigma-Aldrich, ≥98%, USA) was used to measure the quantum yield of the prepared CQDs. Bisphenol A (BPA, $C_{15}H_{16}O_2$, Sigma-Aldrich, ≥99%, USA), hydroquinone ($C_6H_4(OH)_2$, Sigma-Aldrich, ≥99%, USA), benzoic acid ($C_7H_6O_2$, Acros Organics, 99%, Belgium), and naphthalene ($C_{10}H_8$, Duksan, 99%, Korea) were used as target materials of the fluorescence experiments.

2. Syntheses

First, 1,3,6-trinitropyrene, a precursor for the synthesis of CQDs, was prepared according to the literature [26]. Pyrene (2 g) and nitric acid (160 mL) as an oxidizing agent were added to a two-necked flask and stirred. While refluxing the mixture, pyrene was nitrified at 80 °C for 12 hours. The prepared solution was then mixed with distilled water (500 mL). This solution was filtered using a 0.22 μm membrane filter under reduced pressure. The yellow powder separated on the membrane filter was dried overnight at 60 °C to obtain 1,3,6-trinitropyrene.

CQDs were prepared by hydrothermal synthesis method. 1,3,6-Trinitropyrene (0.5 g) and 0.2 M NaOH aqueous solution (100 mL) were mixed and stirred for 10 minutes, and the mixture was dispersed for 2 hours with a sonicator. When a dark yellow homogeneous mixture was made, the solution was transferred to an autoclave and reacted at 200 °C for 10 hours. The mixture was filtered with a 0.22 μm membrane filter under reduced pressure to remove the insoluble carbon compound that does not fluoresce. The filtered

solution was purified by silica gel column chromatography. Silica 60 was used as the stationary phase and ethanol was used as the mobile phase. Ethanol was removed from the separated CQDs using a rotary evaporator at 70 °C. And then, the CQDs were dispersed in distilled water, and stored for the next experiment. The CQD before purification by silica gel column chromatography and the purified CQD were denoted as CD and p-CD, respectively. A schematic of the synthesis procedure of CQDs is shown in the Supporting Information (Fig. S1).

3. Characterization

To check whether 1,3,6-trinitropyrene was well synthesized, the prepared material was analyzed using a nuclear magnetic resonance spectrometer (NMR spectrometer, JEOL, JNM-ECZ500R, Japan) and a high resolution mass spectrometer (HRMS, JEOL, JMS 700, Japan). To confirm the particle shape and size of p-CD, a scanning transmission electron microscope (STEM, Hitachi, HD-2300A, Japan) was used. The structure of p-CD was analyzed using Raman spectroscopy (Thermo Scientific, Nicolet Almega XR, USA). Fourier transform infrared spectrometer (FT-IR, Thermo Scientific, Nicolet iS50, USA) and X-ray photoelectron spectroscopy (XPS, Thermo Fisher, NEXSA, USA) were used to confirm the chemical bonding and surface functional groups of the prepared CQDs.

4. Fluorescence Experiment

Fluorescence-lifetime imaging microscope (FLIM, PicoQuant, Microtime-200, Germany) was used to confirm the quantum yield and excitation dependence of p-CD. The change in fluorescence of p-CD according to the change in BPA concentration was also measured using FLIM. The excitation wavelength of 285 nm was used and the emission wavelength was analyzed in the range of 400 to 700 nm. BPA aqueous solution was prepared at concentrations of 0.2 μM, 0.4 μM, 0.6 μM, 0.8 μM, and 1.0 μM, and p-CD was prepared as an aqueous solution of 0.6 mg/L. Aqueous solution of p-CD (0.5 mL) and the BPA aqueous solution (0.5 mL) were mixed together, and fluorescence was measured immediately after mixing. Since the p-CD aqueous solution and the BPA aqueous solution were mixed in equal amounts, the concentration of the BPA aqueous solution used for fluorescence measurement was diluted to half the concentration of the initially prepared aqueous solution. To confirm whether p-CD selectively causes fluorescence change for BPA, fluorescence changes were also measured in the same manner for polyaromatic compounds including hydroquinone, benzoic acid, and naphthalene, which have similar molecular structures to BPA.

RESULTS AND DISCUSSION

1. Characterization

H NMR analysis result is shown in the Supporting Information (Fig. S2). Seven proton peaks were identified at δ 9.39 (s, 1H), δ 9.20 (d, J=9.5 Hz, 1H), δ 9.14 (d, J=10 Hz, 1H), δ 9.06 (d, J=10 Hz, 1H), δ 8.84 (d, J=10 Hz, 1H), and δ 8.56 (d, J=9.5 Hz, 2H). Proton 2 of 1,3,6-trinitropyrene was located between the electron withdrawing NO_2 groups, so that the chemical shift was the greatest and it was shown as a singlet state. Protons 4, 5, 7, 8, 9, and 10 appeared to be in a doublet state due to adjacent protons, and the coupling constant J value showed constant values of 9.5 Hz and 10 Hz due to the influence of the protons at the ortho position. The H NMR analysis result was found to be consistent with the molecular structure of 1,3,6-trinitropyrene and the literature results [27]. In addition, the mass of the prepared material was measured by a high-resolution mass spectrometer (HRMS) using the electron ionization method, and the result is shown in the Supporting Information (Fig. S3). The molecular formula of 1,3,6-trinitropyrene is $C_{16}H_7N_3O_6$, and the calculated mass-to-charge ratio (m/z) value is 337.2481. In the HRMS measurement, a peak with an m/z value of 337.0335 was confirmed, indicating that 1,3,6-trinitropyrene was well synthesized. Additionally, a small peak due to isotopes was observed at a position where the m/z value was 338.0365. As described here, it was found that 1,3,6-trinitropyrene was successfully prepared from the H NMR and HRMS analysis results.

Particle size and shape of the prepared p-CD were analyzed using STEM. After ultrasonically dispersing of 10 ppm p-CD aqueous solution for 30 seconds, it was measured at 200 kV using a carbon grid, and the result is shown in Fig. 1. The prepared p-CD showed a spherical shape and the particle size was distributed over a wide range with a diameter of 2 to 8 nm. The average particle size was about 5 nm, which is the typical size of carbon dot.

The chemical bonds of 1,3,6-trinitropyrene, a raw material for the synthesis of CQDs, and the prepared CD and p-CD, were analyzed using FT-IR. It was measured using the attenuated total reflectance technique, and a diamond crystal module was used. Fig. 2 shows the results of the FT-IR analyses, which were calibrated ac-

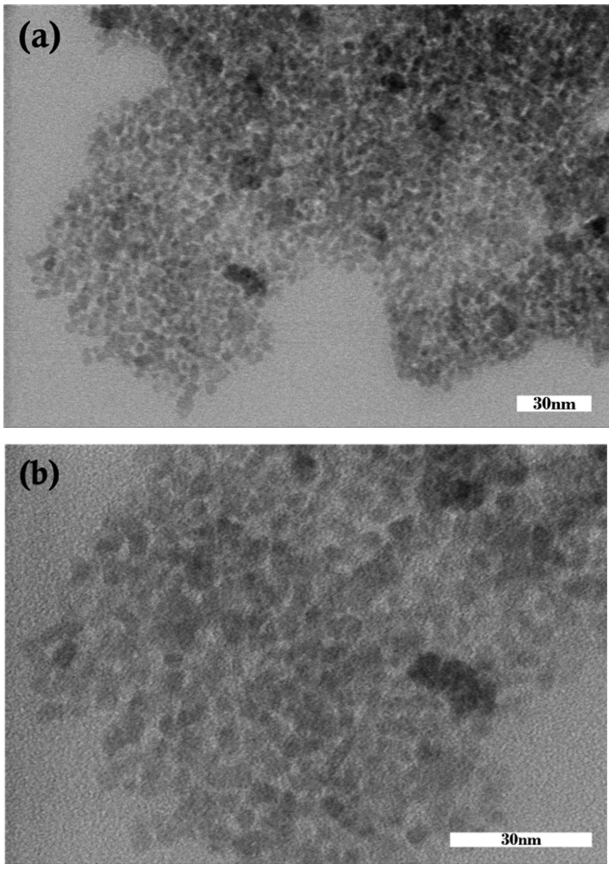

Fig. 1. TEM images of the prepared p-CD ((a) and (b)).

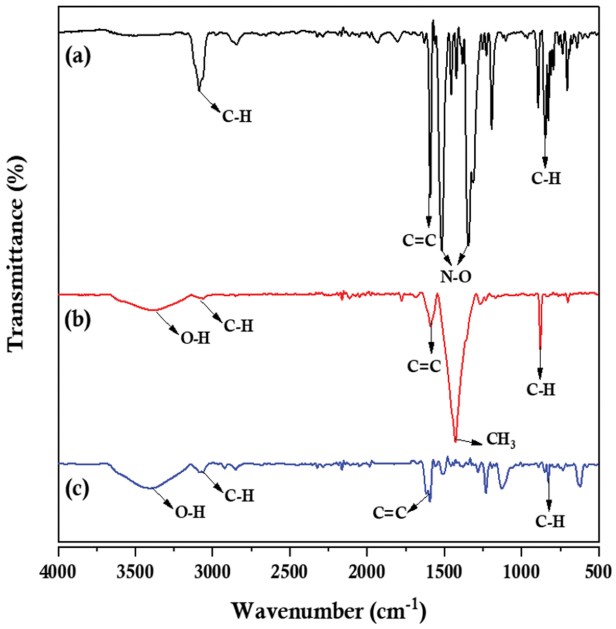

Fig. 2. FT-IR spectra of 1,3,6-trinitropyrene (a), CD (b) and p-CD (c).

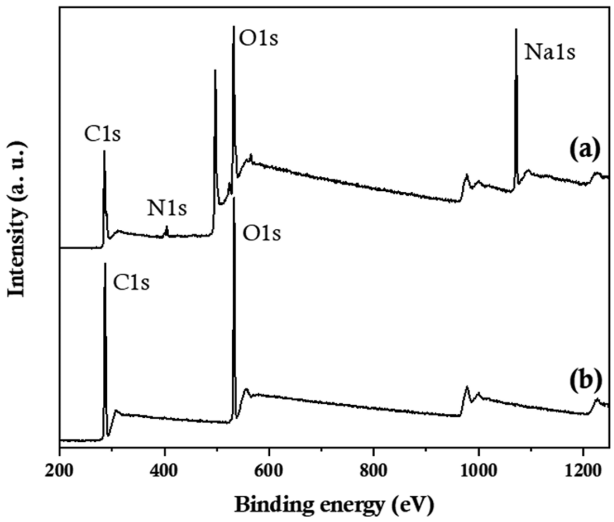

Fig. 3. XPS survey spectra of (a) CD and (b) p-CD.

cording to the characteristics of the diamond crystal. In the measurement of 1,3,6-trinitropyrene, a vibration peak and a stretching peak of C-H were found in the vicinity of 850 cm^{-1} and 3,090 cm^{-1}, respectively (Fig. 2(a)). The peak for C=C due to the aromatic structure of 1,3,6-trinitropyrene was confirmed around 1,591 cm^{-1} [28]. The C-H and C=C peaks were observed in the same positions in all of 1,3,6-trinitropyrene, CD, and p-CD because the prepared CQDs were synthesized while maintaining the aromatic skeleton structure of 1,3,6-trnitropyrene. In addition, N-O peaks, a characteristic peak of 1,3,6-trinitropyrene, were observed in the vicinity of 1,343 cm^{-1} and 1,518 cm^{-1}, indicating that 1,3,6-trinitropyrene was successfully prepared (Fig. 2(a)) [26]. In the CD, an O-H vibration peak was observed around 3,390 cm^{-1}, and strong CH_3 peak was observed around 1,420 cm^{-1} (Fig. 2(b)) [29,30]. However, in p-CD no CH_3 peak was observed near 1,420 cm^{-1}, because unreacted substances or impurities were removed during silica gel column chromatography purification process (Fig. 2(c)). After the purification process, it was confirmed that the O-H peak near 3,390 cm^{-1} became stronger. This implied that p-CD was rich in O-H functional groups as the impurities were removed.

Elemental composition and surface chemical bonding state of CQDs were analyzed using XPS. Elements were analyzed for C, N, O, and Na. Fig. 3 shows the results of the XPS survey spectra for CD and p-CD. Peaks for C1s and N1s were confirmed, respectively, at the binding energies of 284.38 eV and 403.78 eV of the XPS survey spectrum of CD (Fig. 3(a)). The N1s peak, which was weaker than other elements, appeared to be a peak for unreacted 1,3,6-trinitropyrene during the synthesis process. In addition, the Na1s peak identified at 1,072.08 eV appeared to be a peak for sodium salt, a by-product generated during CD production. In the CD survey spectrum, the peak at 497.08 eV appeared to be the Auger peak for Na. As can be seen from the XPS survey spectrum of CD, the CD contained many unreacted products and by-products. These by-products can interfere with the fluorescence properties of CQDs. Therefore, the prepared CQDs must undergo a purification process, for which methods such as column chromatography, dialysis, and HPLC have been usually used. In this work, CD was purified by column chromatography, which is inexpensive and can be performed in a short time compared to other methods [9]. Hydrogen bonds and van der Waals attraction act between CQDs and silica 60, which is a fixed phase of chromatography, so that a component having numerous hydroxyl groups (-OH) stays in the column for a longer time [31]. Using this principle, p-CD rich in hydroxyl groups was selectively separated and purified from CD containing unreacted products and impurities.

In the XPS survey spectrum of p-CD purified by silica gel column chromatography, N1s and Na1s peaks did not appear (Fig. 3(b)). This shows that most of the unreacted product and the sodium byproduct were removed during the purification of CD by silica gel column chromatography. And the absence of the N1s peak in the p-CD survey spectrum shows that NO_2 of 1,3,6-trinitropyrene and OH^- generated from NaOH underwent a nucleophilic substitution reaction during hydrothermal synthesis to form CQDs [26]. To confirm the elemental composition of CD and p-CD, the peak areas of C1s, N1s, and O1s of the XPS survey spectra were measured, and the results are shown in the Supporting Information (Table S1). It was found that most of the impurities including nitrogen were removed during the purification process, showing the decrease of nitrogen content. In addition, since impurities and unreacted products may contain some oxygen compound, the oxygen content seemed to be decreased after the purification process. However, even after purification, p-CD still had a high carbon and oxygen content, implying that p-CD had a large carbon skeleton structure and contained a large number of oxygen-containing functional groups.

The chemical bonds of carbon and oxygen elements were confirmed by analyzing the high-resolution XPS spectra of C1s and O1s of CD and p-CD (Fig. 4). Four peaks were identified in the C1s spectrum of CD. At 284.40 eV, 286.08 eV, and 288.00 eV, C-C

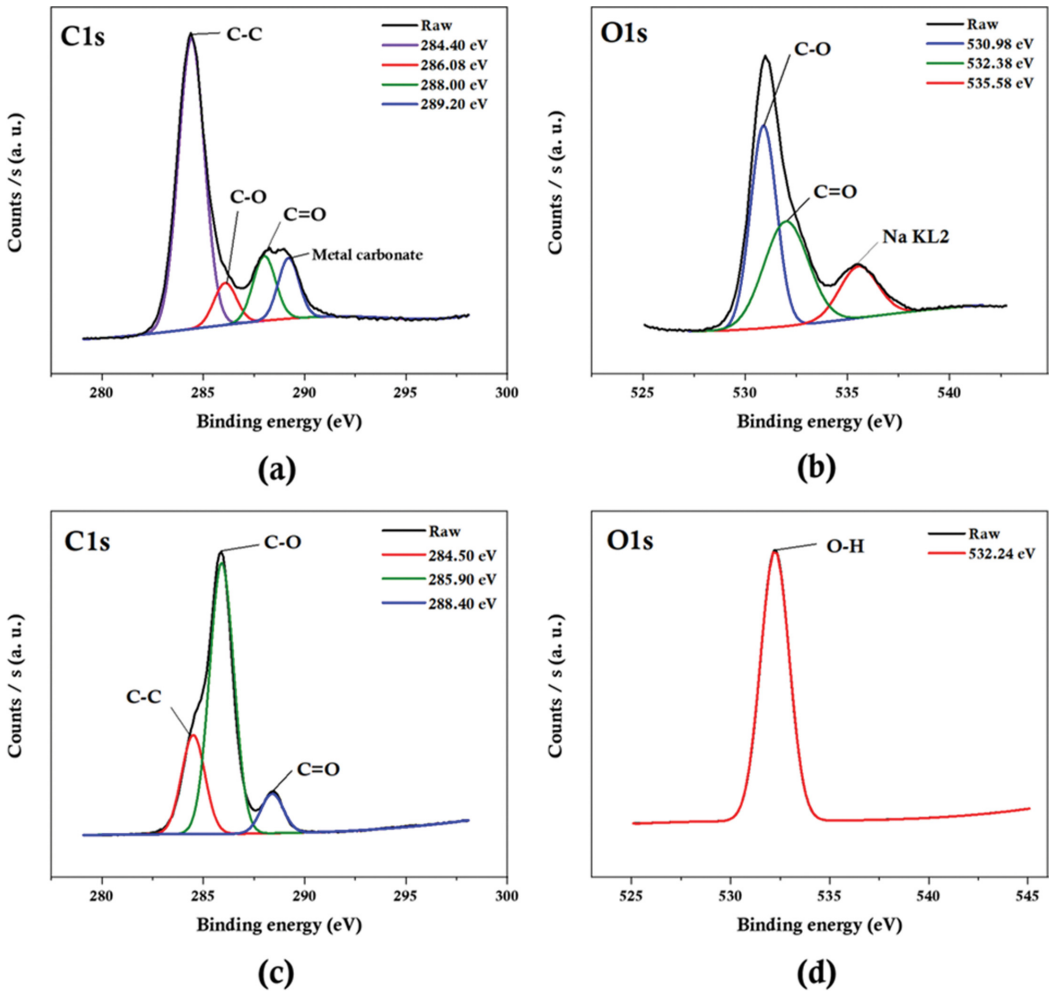

Fig. 4. XPS high resolution C1s and O1s spectra of CD ((a) and (b)) and p-CD ((c) and (d)).

(sp^3), C-O, and C=O bonding peaks were confirmed, respectively. A metal carbonate peak for sodium salt, an impurity produced in the manufacturing process, was confirmed at 289.20 eV. Three peaks were identified in the O1s spectrum including C-O and C=O bonding peaks at 530.98 eV and 532.38 eV, respectively. In addition, Na KL2 peak was confirmed at 535.58 eV. In the C1s spectrum of p-CD, C-C, C-O, and C=O binding peaks were observed at 284.50 eV, 285.90 eV, and 288.40 eV, respectively, in the same manner as the C1s spectrum of CD. And the metal carbonate peak that appeared in C1s spectrum of CD did not appear. In the O1s spectrum of p-CD, only a strong O-H peak was observed at 532.24 eV, confirming that many O-H functional groups exist on the surface of p-CD. From these results, it was found that functional groups with oxygen were abundant on the surface of p-CD [26].

Fig. 5 shows the results of measuring the absorption wavelength of CD and p-CD using an UV-visible spectrometer. The absorption spectra were measured in the range of 200 nm to 800 nm. Comparing the absorption spectrum of CD and that of p-CD, more distinct transition absorption peaks were observed in the spectrum of p-CD. This is thought to be because non-fluorescent substances such as insoluble carbon compounds, sodium salts, and unreacted substances were removed during the purification process. A π-π^* transition absorption peak corresponding to C=C (sp^2) was confirmed near 210 nm in p-CD. Around 270 nm, an n-

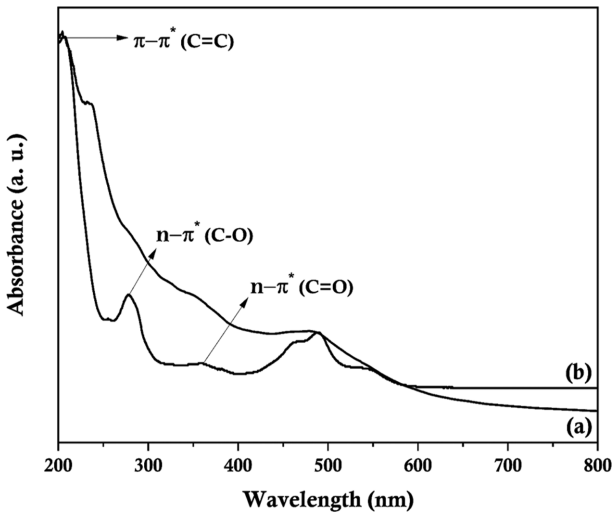

Fig. 5. UV-vis absorbance spectra of CD (a) and p-CD (b).

π^* transition absorption peak corresponding to C-O was confirmed. A weak n-π^* transition absorption peak was also observed around 350 nm, which was thought to be due to the low C=O content [25]. In addition, characteristic absorption spectra due to many surface functional groups of CQDs are shown in the visible region [32]. The strong absorption spectrum at 400 nm to 500 nm appears to be a peak due to the aromatic structure of p-CD [33].

To analyze the structure of p-CD, analysis was performed using Raman spectroscopy. A 532 nm laser was used and the measured Raman spectrum is shown in the Supporting Information (Fig. S4). D band was identified at 1,320 cm^{-1}, indicating that p-CD is an amorphous carbon compound that has a defective and disordered carbon structure [34]. And G band and D′ band appeared around 1,580 cm^{-1} and 1,620 cm^{-1}, respectively. Only G band appears in the perfect graphene structure. However, when graphene has a surface charge, the G band may split and appear as two peaks, G and D′ [35]. From this measurement, it was confirmed that p-CD had an amorphous graphene structure.

2. Fluorescence Experiment

Quantum yield of p-CD was obtained using the relative quantum yield measurement method. The relative method is a method of measuring the quantum yield of a sample based on the quantum yield of a known reference material [36]. The equation for the relative method is as shown below:

$$\Phi_i = \Phi_{st} \times \frac{I_i}{I_{st}} \times \frac{A_{st}}{A_i} \times \frac{n_i^2}{n_{st}^2} \quad (1)$$

In this equation, Φ is the quantum yield, I is the integrated fluorescence intensity, A is the optical density, and n is the refractive index of the solvent. The subscript 'st' refers to a reference standard, and 'i' refers to the sample. L-tryptophan was used as a reference standard. The quantum yield of L-tryptophan aqueous solution at an excitation wavelength of 280 nm is 0.12 [37]. The optical densities (A_i and A_{st}) of p-CD and the standard were measured using an UV-visible spectrometer, and the integrated fluorescence intensities (I_i and I_{st}) of p-CD and the standard were measured using a FLIM. A_i and A_{st} were 0.023 and 0.035, and I_i and I_{st} were 835299.81 and 623994.77, respectively. Water was used as a solvent in both materials, and the same refractive index (1.33) was used in the equation. From the measured values, it was found that the quantum yield of p-CD was 0.13 at the excitation wavelength of 280 nm. Most of the graphene-structured CQDs showed a fluorescence quantum yield of less than 0.15, and the p-CD prepared in this work also showed a similar result [26].

To confirm the excitation dependence of the emission wavelength, the fluorescence intensity of the p-CD aqueous solution was measured at various wavelengths. Excitation wavelengths of 285 nm, 330 nm, 380 nm and 440 nm were used, and the measurement results are shown in Fig. 6. It was confirmed that p-CD had no excitation dependence, as the emission wavelength was the same as 535 nm at all four excitation wavelengths used. In addition, the inset of Fig. 6 shows a photograph when CD and p-CD were irradiated at 365 nm wavelength. It confirmed that the fluorescence of p-CD was clearer and stronger than that of CD. This is presumably because the non-fluorescent materials contained in the CD were removed during the purification process.

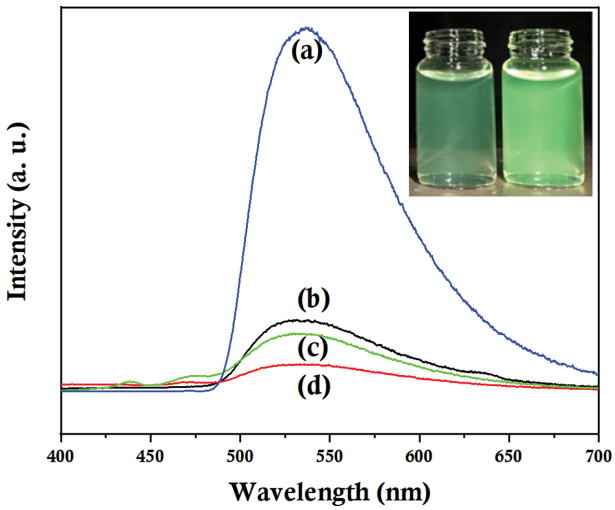

Fig. 6. Fluorescence intensities of p-CD according to the excitation wavelengths of (a) 440 nm, (b) 285 nm, (c) 380 nm and (d) 330 nm (inset: fluorescence photo of CD (left) and p-CD (right) excited by a light source with a wavelength of 365 nm).

The fluorescence change of p-CD was tested in BPA aqueous solution. To set the concentration of p-CD suitable for the fluorescence experiment, fluorescence experiments were performed using p-CD aqueous solutions of various concentrations from 0.6 mg/L to 1.0 mg/L. In all samples, as the concentration of BPA increased, the fluorescence intensity of p-CD increased. However, the linearity of the change in fluorescence intensity with respect to the concentration of BPA was best when p-CD was 0.6 mg/L (Data not shown here). Therefore, in this work, the concentration of p-CD aqueous solution was fixed at 0.6 mg/L.

The fluorescence intensity of p-CD increased linearly as the BPA concentration increased. The fluorescence spectra measured

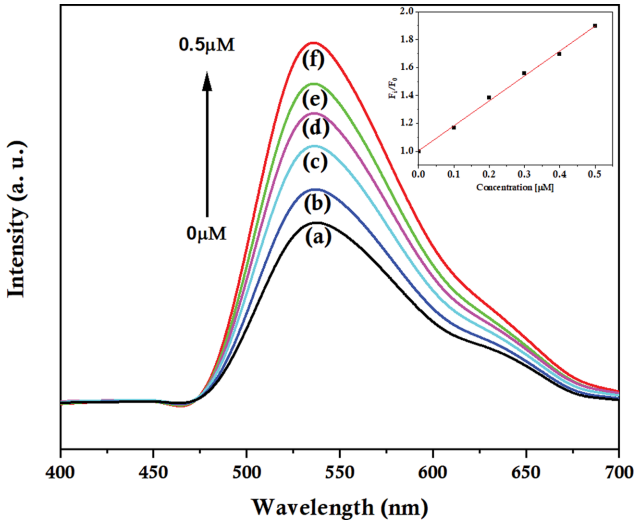

Fig. 7. Fluorescence intensities of p-CD according to the BPA concentrations of (a) 0 μM, (b) 0.1 μM, (c) 0.2 μM, (d) 0.3 μM, (e) 0.4 μM and (f) 0.5 μM (inset: relative fluorescence intensity (F_i/F_0) change according to BPA concentrations).

at the excitation wavelength of 285 nm while changing the concentration of BPA are shown in Fig. 7. In all fluorescence spectra, the maximum value of fluorescence appeared at 535 nm. Relative fluorescence intensity, F_i/F_0, was calculated using the measured value at 535 nm to confirm the linearity of the change in fluorescence intensity with respect to the BPA concentration. F_0 is the fluorescence intensity in the absence of BPA and F_i is the fluorescence intensity in the presence of BPA, respectively. When the linear equation was applied, the R^2 value was very high at 0.99749. It was found that the fluorescence intensity of p-CD had high linearity in the concentration range of BPA used in this work (0.0 μM-0.5 μM). However, when the concentration of BPA was increased to 1.0 μM, it was observed that the fluorescence of p-CD was quenched and decreased (Data not shown here). This seems to be a result of aggregation between p-CD and high concentration of BPA or energy transfer by interaction between BPA molecules. The cause of this phenomenon is not clear, and further research needs to be performed.

Experiments were also performed to find the fluorescence mechanism of detecting BPA using p-CD. Sensing mechanisms using fluorescence of CQDs include static quenching, dynamic quenching, inner filter effect, Forster resonance energy transfer (FRET) and photoinduced electron transfer [22]. Among them, FRET is a non-radiative energy transfer process by dipole-dipole interaction between donor and acceptor molecules. FRET depends on the arrangement of molecules and the distance between them. When the distance between the donor molecule and the acceptor molecule is less than 10 nm, energy can be transferred from the donor molecule to the acceptor molecule. The transferred energy can be expressed as fluorescence [38].

The excitation wavelength spectrum for emission of 550 nm fluorescence of p-CD was measured and compared with the fluorescence emission spectrum when BPA was excited at a wavelength of 285 nm (Fig. 8). As shown in the figure, the excitation wavelength for fluorescence emission of p-CD and the fluorescence emission wavelength of BPA overlap in the range of 300 nm-450 nm. From this result, it can be inferred that the fluorescence emitted from BPA acts to excite the fluorescence emission of p-CD by

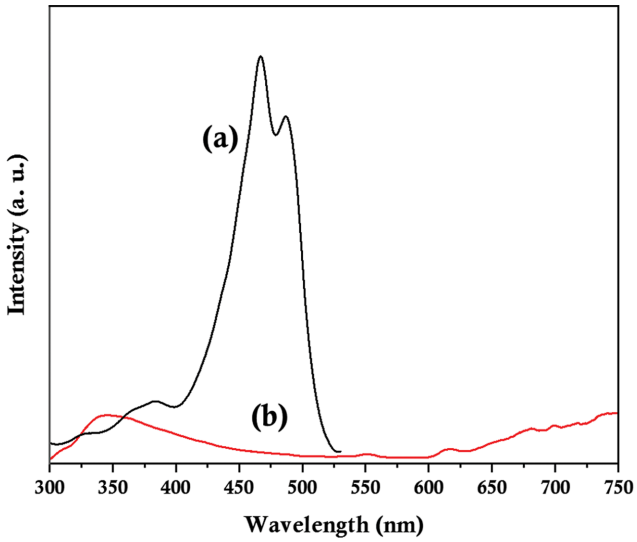

Fig. 8. (a) Excitation wavelength spectrum for emission of 550 nm fluorescence of p-CD and (b) emission spectrum of BPA excited at 285 nm.

the energy transfer from BPA to p-CD. For energy transfer between two molecules, the distance between the two molecules should be close to 10 nm or less. The p-CD prepared in this work has a graphene structure and has many hydroxyl groups, so it can adsorb BPA with benzene ring and hydroxyl group through π-π interactions and hydrogen bonding [39]. Therefore, the distance between the two molecules might become closer to less than 10 nm, and it seems that FRET occurred between p-CD and BPA. A schematic diagram of BPA detection by p-CD is shown in Fig. 9. As the BPA concentration increases, the fluorescence emission of BPA becomes stronger in the wavelength region, overlapping the excitation spectrum of p-CD. As a result, more energy transfer can occur between p-CD and BPA, resulting in the increase of the fluorescence intensity of p-CD with the increase of the concentration of BPA.

Three aromatic compounds having a similar structure to BPA such as benzoic acid, hydroquinone, and naphthalene were selected

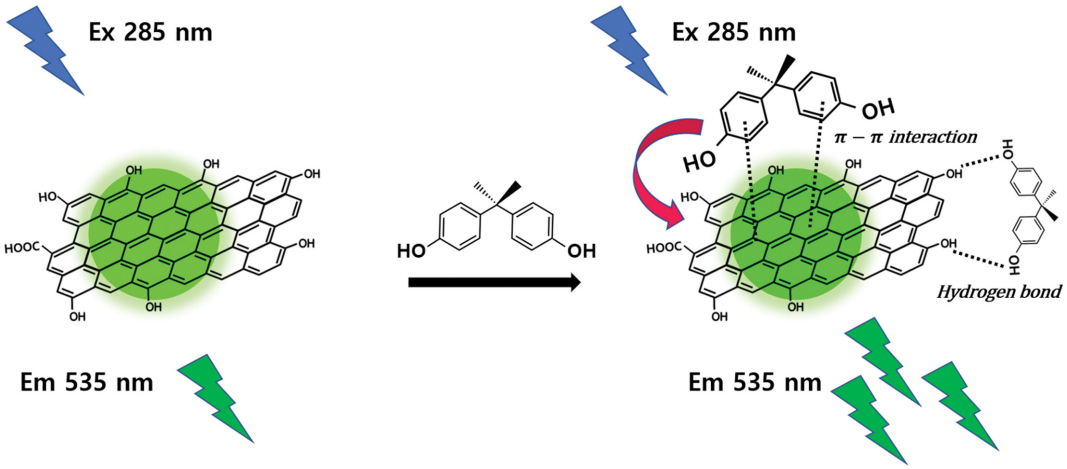

Fig. 9. Schematic of BPA detection mechanism by p-CD.

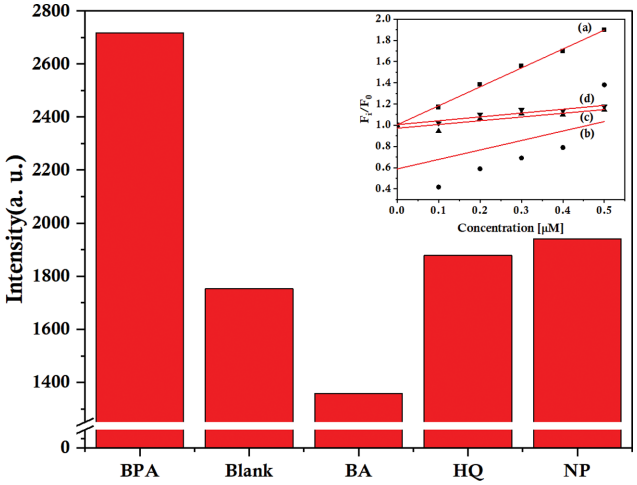

Fig. 10. Fluorescence intensities in the absence (Blank) and presence of the target substances including BPA, benzoic acid (BA), hydroquinone (HQ), and naphthalene (NP) (inset: relative fluorescence intensity (F_f/F_0) changes according to the target substance concentrations including (a) BPA, (b) BA, (c) HQ, and (d) NP).

and used in the fluorescence experiments to determine whether p-CD had detection selectivity for BPA. Three target materials were prepared at concentrations of 0.2 μM, 0.4 μM, 0.6 μM, 0.8 μM, and 1.0 μM, and fluorescence intensity was measured by mixing the aqueous solution of the target material (0.5 mL) and p-CD at a concentration of 0.6 mg/L (0.5 mL). To compare the change in fluorescence intensity of p-CD according to the target material, the average value of the fluorescence intensities measured at five concentrations of each target substance was calculated and shown in Fig. 10 [23]. In the figure, "Blank" means the fluorescence intensity measured when p-CD and distilled water are mixed. When comparing the results of the BPA and other target material, it was confirmed that the fluorescence intensity was clearly high in BPA aqueous solution. The increase in fluorescence intensity in BPA was more than five-times larger than that in other target materials. In the case of benzoic acid, the fluorescence was decreased, and the fluorescence intensities of hydroquinone and naphthalene were almost similar to that of Blank. The relative fluorescence intensity changes according to the concentrations of the target substances are shown in the inset of Fig. 10. As shown, the fluorescence change according to the concentration in the aqueous BPA solution was relatively large. However, in the other target substances, fluorescence decreased (benzoic acid) or fluorescence change hardly occurred (hydroquinone and naphthalene). This experiment confirmed that p-CD has the potential as a selective detection sensor for BPA. The reason p-CD is selective for BPA over other target substances seems to be due to the interaction between BPA and p-CD. BPA has two aromatic rings and two hydroxyl groups. Therefore, the π-π interaction and hydrogen bonding can occur strongly between BPA and p-CD. However, benzoic acid and hydroquinone have only one aromatic ring, and each has a carboxyl group and a hydroxyl group, respectively. Thus, the two compounds appear to have weaker π-π interactions with p-CD than BPA. Naphthalene has two aromatic rings, but it does not have a hydroxyl group, so hydrogen bonding with p-CD cannot occur. For this reason, p-CD appears to have higher detection selectivity for BPA than benzoic acid, hydroquinone, and naphthalene, which have similar molecular structures to BPA.

CONCLUSIONS

CQD was synthesized by simple hydrothermal synthesis using 1,3,6-trinitropyrene and sodium hydroxide aqueous solution to selectively detect BPA in aqueous solution. CD containing unreacted material and impurities was separated and purified by silica gel column chromatography to obtain p-CD. The prepared p-CD was characterized, and it was confirmed that p-CD could detect BPA by increasing fluorescence with the increase of BPA concentration via the FRET mechanism. In addition, by comparative experiments on the target substances having a similar structure to BPA, it was confirmed that p-CD had the potential as a selective detection sensor for BPA in aqueous solution.

ACKNOWLEDGEMENT

This work was supported by the National Research Foundation of Korea (NRF) grant funded by the Korea government (MSIT) (No. 2020R1F1A1048770).

SUPPORTING INFORMATION

Additional information as noted in the text. This information is available via the Internet at http://www.springer.com/chemistry/journal/11814.

REFERENCES

1. A. Bhatnagar and I. Anastopoulos, *Chemosphere*, **168**, 885 (2017).
2. J. Yoo, J. Na and J. Jung, *Ecol. Resil. Infrastruct.*, **6**(2), 128 (2019).
3. C. Grignon, N. Venisse, S. Rouillon, B. Brunet, A. Bacle, S. Thevenot, V. Migeot and A. Dupuis, *Anal. Bioanal. Chem.*, **408**(9), 2255 (2016).
4. H. S. Chang, K. H. Choo, B. Lee and S. J. Choi, *J. Hazard. Mater.*, **172**(1), 1 (2009).
5. F. Xue, J. Wu, H. Chu, Z. Mei, Y. Ye, J. Liu, R. Zhang, C. Peng, L. Zheng and W. Chen, *Microchim. Acta*, **180**, 109 (2013).
6. Y. Lu, L. Doan, A. Bafana, G. Yu, C. Jeffryes, T. Benson, S. Wei and E. K. Wujcik, in *Polymer-based multifunctional nanocomposites and their applications*, K. Song, C. Liu and J. Z. Guo (Ed.), Elsevier, Amsterdam (2019).
7. M. L. Liu, B. B. Chen, C. M. Li and C. Z. Huang, *Green Chem.*, **21**(3), 449 (2019).
8. M. R. Wilner and P. J. Viksland, *J. Nanobiotechnol.*, **16**(1), 1 (2018).
9. A. Koutsioukis, A. Akouros, R. Zboril and V. Georgakilas, *Nanoscale*, **10**(24), 11293 (2018).
10. G. S. Das, J. P. Shim, A. Bhatnagar, K. M. Tripathi and T. Kim, *Sci. Rep.*, **9**(1), 1 (2019).
11. D. Yoo, Y. Park, B. Cheon and M. Park, *Nanoscale Res. Lett.*, **14**(1), 1 (2019).
12. X. Zhang, M. Jiang, N. Niu, Z. Chen, S. Li, S. Liu and J. Li, *Chem-*

SusChem, **11**(1), 11 (2018).
13. H. Yang, L. He, S. Pan, H. Liu and X. Hu, *Spectroc. Acta Pt. A-Molec. Biomolec. Spectr.*, **210**, 111 (2019).
14. Y. Yan, J. H. Liu, R. S. Li, Y. F. Li, C. Z. Huang and S. J. Zhen, *Anal. Chim. Acta*, **1063**, 144 (2019).
15. H. Xu, X. Yang, G. Li, C. Zhao and X. Liao, *J. Agric. Food Chem.*, **63**(30), 6707 (2015).
16. M. Ghereghlou, A. A. Esmaeili and M. Darroudi, *J. Fluoresc.*, **31**(1), 185 (2021).
17. M. Xue, M. Zou, J. Zhao, Z. Zhan and S. Zhao, *J. Mat. Chem. B*, **3**(33), 6783 (2015).
18. Q. Wang, X. Liu, L. Zhang and Y. Lv, *Analyst,* **137**(22), 5392 (2012).
19. S. A. Nsibande and P. B. C. Forbes, *RSC Adv.*, **10**(21), 12119 (2020).
20. K. K. Chan, S. H. K. Yap and K. T. Yong, *Nano-Micro Lett.*, **10**(4), 1 (2018).
21. F. Yan, Z. Sun, H. Zhang, X. Sun, Y. Jiang and Z. Bai, *Microchim. Acta*, **186**(8), 1 (2019).
22. F. Zu, F. Yan, Z. Bai, J. Xu, Y. Wang, Y. Huang and X. Zhou, *Microchim. Acta*, **184**(7), 1899 (2017).
23. L. Wang, H. X. Cao, C. G. Pan, Y. S. He, H. F. Liu, L. H. Zhou, C. Q. Li and G. X. Liang, *Microchim. Acta*, **186**(1), 1 (2019).
24. G. Liu, Z. Chen, X. Jiang, D. Q. Feng, J. Zhao, D. Fan and W. Wang, *Sens. Actuators B-Chem.*, **228**, 302 (2016).
25. D. Zhao, X. Liu, C. Wei, Y. Qu, X. Xiao and H. Cheng, *RSC Adv.*, **9**(51), 29533 (2019).
26. L. Wang, Y. Wang, T. Xu, H. Liao, C. Yao, Y. Liu, Z. Li, Z. Chen, D. Pan, L. Sun and M. Wu, *Nat. Commun.*, **5**, 1 (2014).
27. S. Kaplan, *Org. Mag. Res.*, **15**(2), 197 (1981).
28. J. R. A. Cosme, H. E. Bryant and F. Claeyssens, *PloS One*, **14**(7), e0220210 (2019).
29. S. Chandra, S. Pradhan, S. Mitra, P. Patra, A. Bhattacharya, P. Pramanik and A. Goswami, *Nanoscale*, **6**(7), 3647 (2014).
30. R. S. D. Costa, W. F. D. Cunha, N. S. Pereira and A. M. Ceschin, *Materials*, **11**(9), 1492 (2018).
31. V. Hinterberger, C. Damm, P. Haines, D. M. Guldi and W. Peukert, *Nanoscale*, **11**(17), 8464 (2019).
32. M. Y. Pudza, Z. Z. Abidin, S. A. Rashid, F. M. Yasin, A. S. M. Noor and M. A. Issa, *Nanomaterials*, **10**(2), 315 (2020).
33. W. Wang, Y. Li, L. Cheng, Z. Cao and W. Liu, *J. Mat. Chem. B*, **2**(1), 46 (2014).
34. C. Reckmeier, J. Schneider, A. Susha and A. Rogach, *Opt. Express*, **24**(2), A312 (2016).
35. Z. Yan and A. R. Barron, in *Nanomaterials and nanotechnology*, A. R. Barron (Ed.), OpenStax CNX, Texas (2015).
36. R. E. D. Araujo and C. T. Dominguez, in *Quantum dots*, A. Fontes and B. Santos (Ed.), Humana, New York (2020).
37. A. M. Brouwer, *Pure Appl. Chem.*, **83**(12), 2213 (2011).
38. L. Wu, C. Huang, B. Emery, A. C. Sedgwick, S. D. Bull, X. P. He, H. Tian, J. Yoon, J. L. Sessler and T. D. James, *Chem. Soc. Rev.*, **49**(15), 5110 (2020).
39. J. Xu, L. Wang and Y. Zhu, *Langmuir*, **28**(22), 8418 (2012).

Supporting Information

Synthesis of a fluorescence sensor based on carbon quantum dots for detection of bisphenol A in aqueous solution

Eunbi Hwang and Byunghwan Lee†

Department of Chemical Engineering, Keimyung University, 1095 Dalgubeoldaero, Dalseo-gu, Daegu 42601, Korea
(*Received 26 July 2021 • Revised 4 October 2021 • Accepted 19 October 2021*)

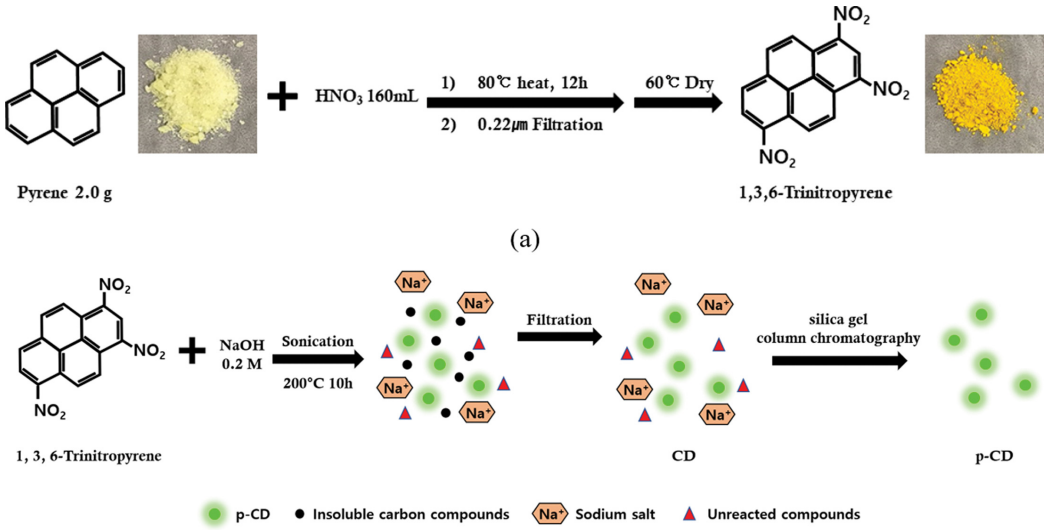

Fig. S1. Synthesis procedure of 1,3,6-trinitropyrene (a) and p-CD (b).

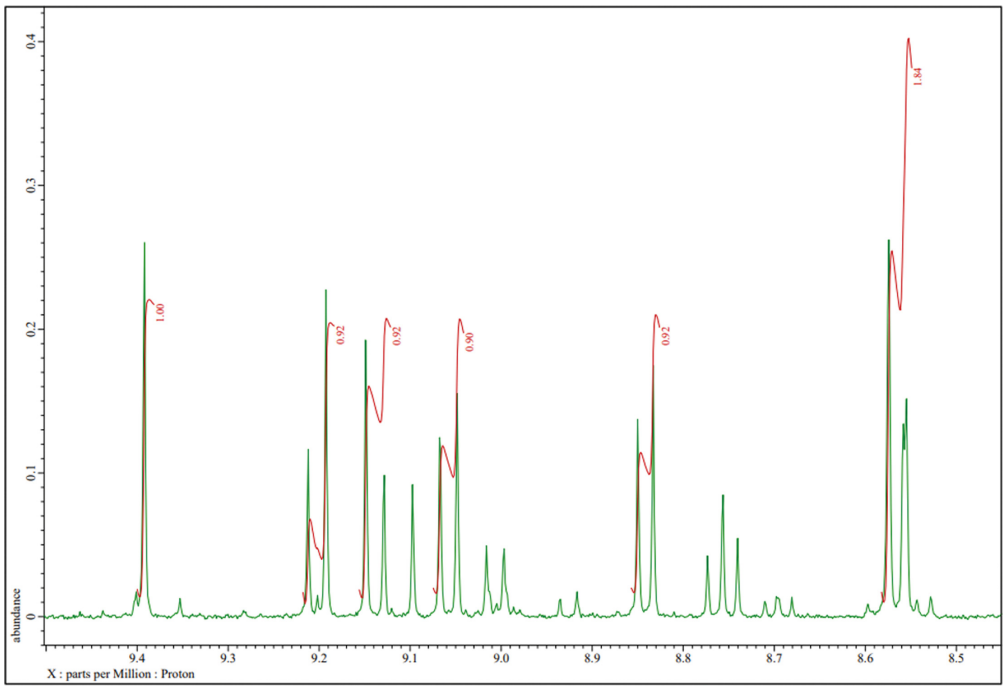

Fig. S2. H NMR spectrum of the 1,3,6-trinitropyrene prepared.

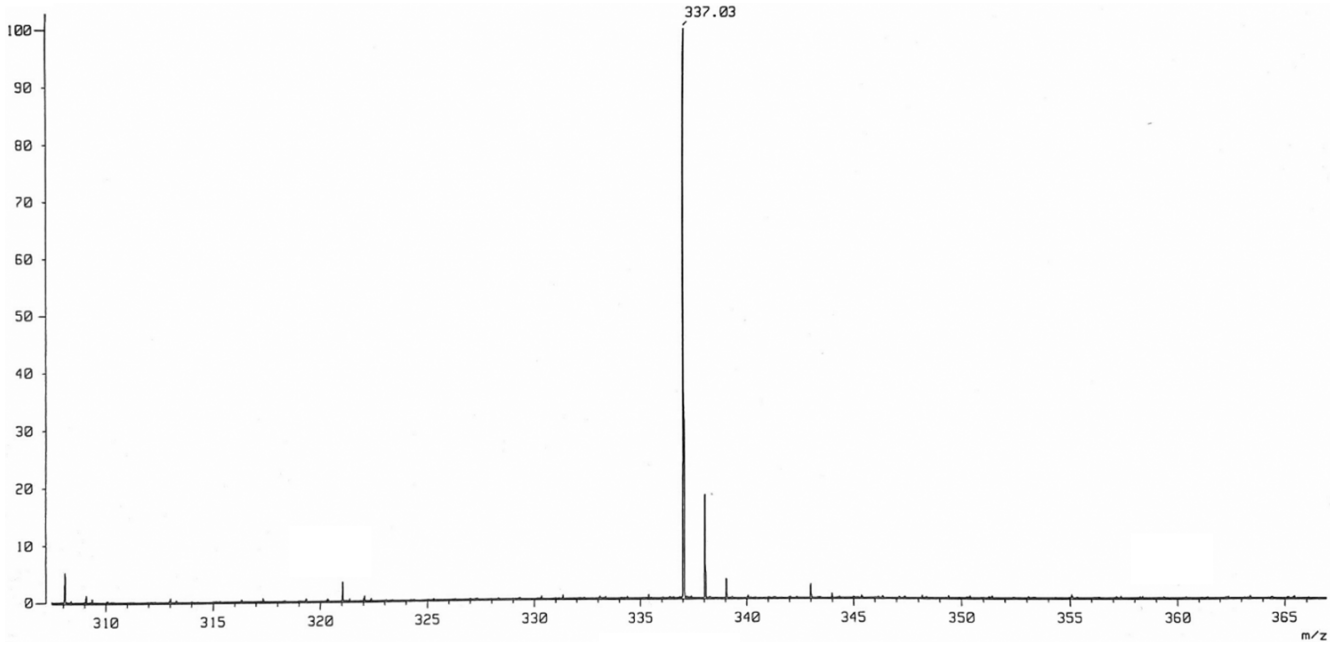

Fig. S3. HRMS spectrum of the 1,3,6-trinitropyrene prepared.

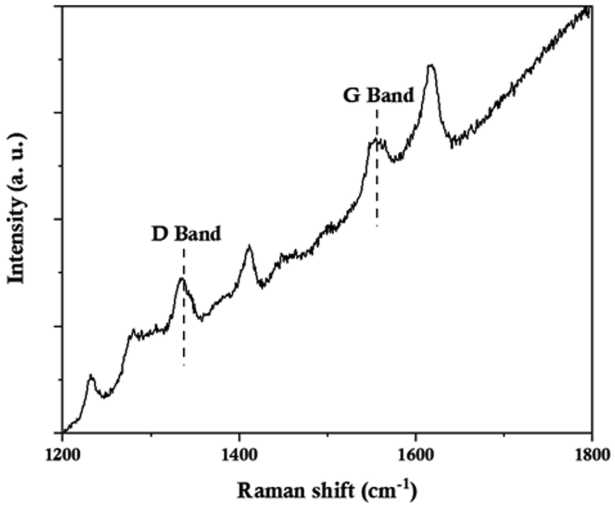

Fig. S4. Raman spectrum of p-CD.

Table S1. Atomic percentages of elements in CD and p-CD

Sample	Element	Atomic percentage (%)
CD	C	57.34
	O	38.27
	N	4.38
p-CD	C	67.62
	O	31.97
	N	0.41